CHINESE OPTICS LETTERS

Vol. 20, No. 3 | March 2022

Autostereoscopic display with bicylindrical lens based on temporal-spatial multiplexing

Xueling Li (李雪玲) and Yuanqing Wang (王元庆)*

School of Electronic Science and Engineering, Nanjing University, Nanjing 210023, China

*Corresponding author: yqwang@nju.edu.cn

Received November 7, 2021 | Accepted December 29, 2021 | Posted Online January 26, 2022

An autostereoscopic display system with a bicylindrical lens based on temporal-spatial multiplexing technique is introduced in this paper. The system comprises a directional scanning backlight, a liquid crystal display panel with high refreshing rate, and an eye tracking device. The directional scanning backlight consists of an LED board, two lenticular lens arrays with matching periods, a parallax barrier film, and other optical films. One of the lenticular lenses is a bicylindrical lens designed to reduce aberration, hence achieving better image quality. A prototype is set up based on the proposed structure. A series of experiments are conducted, and the overall performance of the prototype is evaluated. The LEDs are divided into 10 groups that form 10 view zones. On the one hand, it achieves full resolution in both 2D and 3D display modes. On the other hand, the viewing angle is increased to ±26 deg. Most importantly, the crosstalk is low. The minimum crosstalk is 6%, and the maximum crosstalk is 8.8% at a viewing angle of ±22 deg.

Keywords: directional backlight; 3D display; temporal-spatial multiplexing.

DOI: 10.3788/COL202220.033301

1. Introduction

Autostereoscopic display has a thriving prospect in many research areas[1] for its more comfortable visual effect over stereoscopic display with auxiliary glasses[2–4]. Several approaches are adopted to implement an autostereoscopic display system. One is spatial multiplexing using parallax barriers[5–9] or lenticular lenses[10–13] to separate parallax images and project them into different positions. This technique stands out for its easy realization on common flat panel display. However, high resolution and large viewing angle have been a major challenge, because horizontal resolution reduces with the increase of the view point. Besides that, the balance of horizontal and vertical resolution is compromised as well.

To improve the performance of autostereoscopic display systems, a temporal-spatial multiplexing technique is introduced. It usually contains a directional backlight unit[14–18], which projects light to different view zones, and an liquid crystal display (LCD) panel with high refreshing rate that displays a pair of parallax images frame by frame. It realizes the fine stereo effect of low crosstalk as well as wide viewing angle and resolution consistency.

We propose a temporal-spatial multiplexed autostereoscopic display system in this paper. The system consists of a directional scanning backlight, a LCD panel, and an eye tracking device. To correct optical aberration, a bicylindrical lens is specially designed for the directional backlight module. In this prototype, 10 view zones are available. The minimum crosstalk is 6%, and the viewing angle is ±26 deg.

2. System Design and Analysis

The overall configuration of the temporal-spatial multiplexed autostereoscopic display system consists of the following parts: directional backlight module, backlight control unit (BLCU), LCD panel of high refreshing rate, and eye tracking device. The eye tracking device obtains the viewers' left and right eye positions in real time, sending them back to the BLCU, where the backlight control signal (BLCS) is generated. The directional backlight module produces display modes accordingly. This progress is shown in Fig. 1(a). Channel separation, as the core technology of autostereoscopic display, is realized through temporal-spatial multiplexing. The left and right images are displayed by the LCD with full resolution frame by frame, and they are projected by the directional backlight module alternatively to the corresponding eye position. To do that, the directional backlight has to be in synchronization with the LCD panel. This principle can be illustrated in Fig. 1(b). For example, under 3D mode, if the LCD is displaying the left image during frame n, the directional backlight operates in mode M and projects the left image to where the left eye locates. During the next frame $n+1$, the LCD is displaying the right image, and the directional backlight changes its mode to M', which projects the right image to the

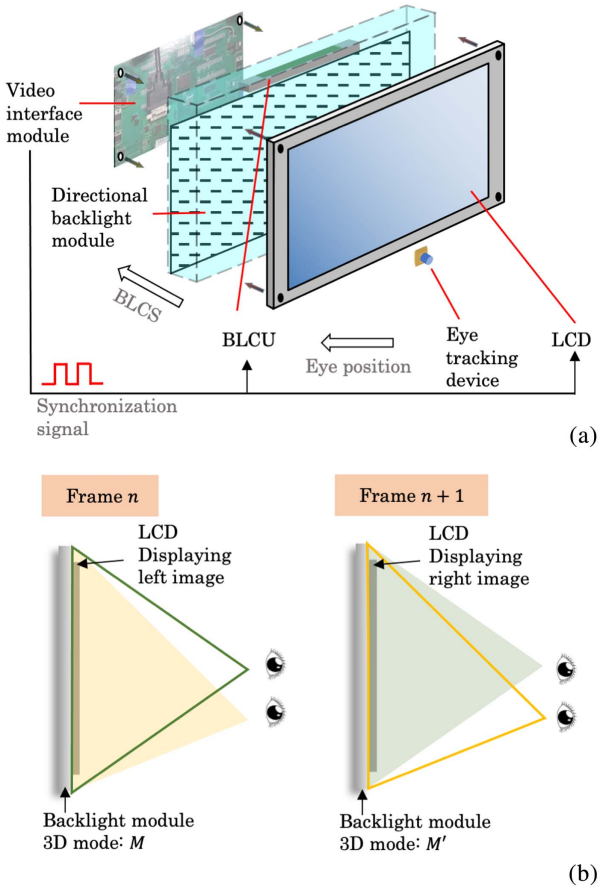

Fig. 1. (a) Overall structure and signal control of the system. (b) Temporal-spatial multiplexing technique.

right eye. Hence, the right eye and left eye are able to perceive different images, and this achieves channel separation. By adopting the temporal-spatial multiplexing technique, full resolution autostereoscopic display can be realized, both in time and space domains. In addition, to further reduce crosstalk, a scanning backlight is adopted in the system. The scanning backlight scheme is introduced in detail in Ref. [19].

2.1. Optical structure

The structure of the designed directional backlight module is illustrated in Fig. 2. The main components include the backlight board, bicylindrical lens array (LLA1), lenticular lens array (LLA2), parallax barrier, and other optical films. The backlight board is placed on the focal plane of LLA1. They are divided into N groups, and each group of LEDs is designated for one view zone. Clearly, each view zone contains light intensity contributed by multiple LEDs. Different groups of LEDs converging to different view zones enable multiple users to watch and provide excellent motion parallax, which is also a valuable merit.

Lenses of LLA1 can refract different groups of LEDs to parallel light of different angles. The two LLAs are placed with their cylindrical surface facing each other. Different angles of parallel light converge into light strips at different positions after LLA2.

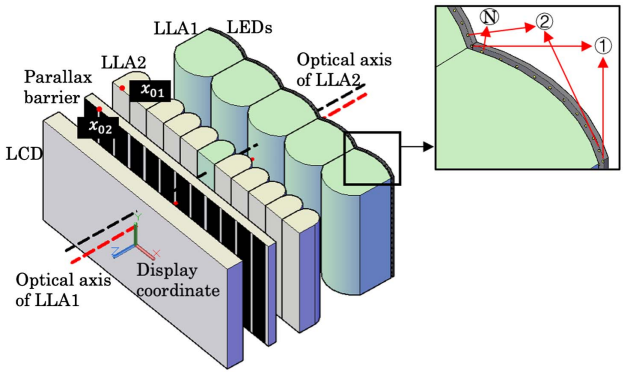

Fig. 2. Structure of the designed directional backlight module.

The parallax barrier is set with an optical interval of d to the focal plane of LLA2 so that light strips can be projected to form view zones.

2.1.1. Design of bicylindrical lens

To form light strips with small width after LLA2, the parallelism of the incident light is important. Ideally, parallel light refracted by the cylindrical lens will form a convergence point on the focal plane. The positions of the convergence points vary on the focal plane with the angle of the incident light. However, in reality, the aberration of the lens has a great influence on the convergence of parallel light. Due to aberration, the incident parallel light with larger angle will not converge to a single point. The equivalent converging point is away from the focal plane, or, in other words, the focal plane is a curved plane rather than a flat one. So, according to optical path reversibility, in order to obtain parallel light, the curvature of the focal plane needs to be determined. As shown in Fig. 3(a), assume O_1 is the original point, $Q_i(x_i,y_i)$ is a point on the curved focal plane, $P_j(x_j,y_j)$ is the exit point on the cylindrical surface of the lenticular lens, and U_{ij} is the actual angle of refracted light with regard to the incident light ray Q_iP_j, where $i = 1, 2, \ldots, N$ is the tag of the simulated point light source located on the focal plane, $j = 1, 2, \ldots, M$

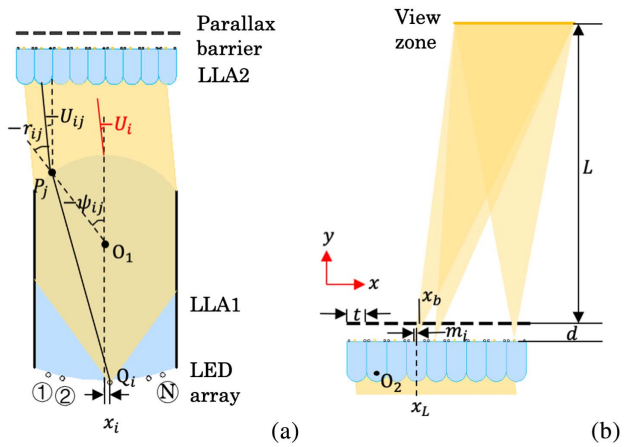

Fig. 3. (a) Design of LLA1. (b) The formation of view zones.

is the tag of simulated points on the exit cylindrical surface. U_i is the angle of the outgoing parallel light requested in ideal conditions. The target of optimization can be described as Eq. (1):

$$\mathrm{rms}^2 = \frac{1}{M}\sum_{i=1}^{M}(U_{ij} - U_i)^2. \tag{1}$$

In this way, the coordinate of the light source that forms parallel light of angle U_i can be determined. Figure 3(a) illustrates the relationship between U_{ij} and the incident light. For each incident light ray, the corresponding angle of refracted light is $U_{ij} = \psi_{ij} - r_{ij}$, where r_{ij} denotes the refraction angle, and ψ_{ij} denotes the angle between the normal and the optical axis. Equations (2) and (3) are the expressions of r_{ij} and ψ_{ij} respectively:

$$r_{ij} = \arcsin\left\{n^* \sin\left[\arccos\left(\frac{P_jQ_i \cdot P_jO}{|P_jQ_i|^*|P_jO|}\right)\right]\right\}, \tag{2}$$

$$\psi_{ij} = \arccos\frac{x_j}{r}. \tag{3}$$

For all the symbols of parameters mentioned in the above formulas, they should be added with a minus sign according to the rules while calculating.

The coordinates of Q_i can be calculated by genetic algorithm. $\frac{1}{\mathrm{rms}^2}$ is set to be the fitness function of the genetic algorithm. With larger value of the fitness function, the angles of the simulated light rays are closer to the ideal angle. Apparently, the surface determined by a series of Q_i is a curved surface that can be approximated as a cylinder.

2.1.2. Principle of the optical imaging

As shown in Fig. 3(a), for N different view zones, on the back of each lens of LLA1, there are N LEDs numbered as ① to ⑧. Since the optical structure only modulates light along the x axis, consider that the ith LED is placed x_i away from the main optical axis of LLA1. f_1 is the focal length of LLA1, and thus the angle of the refractive parallel light rays can be described by Eq. (4):

$$\tan(-U_i) = \frac{x_i}{f_1}. \tag{4}$$

Parallel light focused by LLA2 forms light strips on the focal plane of LLA2, as demonstrated in Fig. 3(b). f_2 is the focal length of LLA2. Therefore, the relative position m_i between the light strip and the main optical axis of LLA2 can be described according to U_i and f_2 as Eq. (5):

$$m_i = (\tan\ U_i) \times f_2 = -\frac{x_i}{f_1} \times f_2. \tag{5}$$

The procedure to determine view zone position X_i (under display coordinate) is as follows. The coordinate of the light strip is $x_l = x_L + m_i$, in which $x_L = x_{01} + k^*p$ is the display coordinate of the principal optical axis of the corresponding lens. The position of the corresponding barrier opening under the display coordinate is $x_b = x_{02} + k^*t$. In the above equations, x_{01} and x_{02} are the starting positions of LLA2 and the parallax barrier, respectively, p and t are the periods of LLA2 and the parallax barrier, respectively, and k is the number of basic units. Suppose $\Delta = x_b - x_l$. Then, according to triangle similarity, the view zone position can be calculated by Eq. (6):

$$X_i = \frac{L}{d} \cdot \Delta + x_b, \tag{6}$$

where L is the viewing distance, and d is the optical interval between the light strips and the parallax barrier. Define the optical magnification factor $\beta_1 = \frac{f_2}{f_1} = \frac{p}{q}$, where q is the period of LLA1, and $\beta_2 = \frac{L}{d}$. According to Eqs. (5) and (6), we have Eq. (7):

$$X_i = (\beta_2 + 1)x_b - \beta_2(x_L - \beta_1 x_i). \tag{7}$$

The center distance of view zones formed by adjacent LEDs is supposed to be Eq. (8):

$$\begin{aligned} S &= |X_{i+1} - X_i| = |(\beta_2 + 1)t - \beta_2 p - \beta_2\beta_1(x_{i+1} - x_i)| \\ &= |\beta_2\beta_1(x_{i+1} - x_i)|. \end{aligned} \tag{8}$$

The relationship between t and p is $p = (1 + \frac{1}{\beta_2})t$. Normally, interpupillary distance E is 60–65 mm, so it should be the maximum of S to realize proper motion parallax.

E is also the width of the view zone. Assuming that the width of the light strip can be ignored, the width of the slit is $w = \frac{d}{d+L}E = \frac{1}{1+\beta_2}E$. Because β_2 is rather large, w is quite small. However, the width of the light strip is not ideal, meaning that w has to be smaller than the theoretical value to keep E under the ideal value. Hence, in order to have bigger w, which equals higher light efficiency, the width of the light strip needs to be small. Hence, the parallelism of light after LLA1 has to be guaranteed, and the design of the bicylindrical lens is necessary.

2.2. Directional backlight controlled by eye tracking device

In order to project correct image information to the corresponding eye location, a high-speed real-time eye tracking device is introduced into the autostereoscopic display system.

The system is composed of a low-resolution thermal infrared (IR) camera, a high-resolution RGB camera, and an industrial computer. Since the human face is very prominent in the IR image, it is easier and faster to detect human faces with an IR camera. Then, the detected human face information can be used to guide the industrial computer to locate eye position in the RGB camera. With IR guiding, the time of detecting eye positions in RGB images can be greatly reduced. Assume the pixel coordinate of the eye position detected in the RGB image is $P_r^p = (x_{\mathrm{er}}^a, y_{\mathrm{er}}^a)$, where $a \in \{1,2\}$, $a = 1$ represents the left eye, $a = 2$ represents the right eye, and r denotes the rth candidate region (CR) in the RGB image. Assume the world coordinate

of the eye position is $P_r^w = (X_r^a, Y_r^a, z)$, where z is the fixed distance from the viewing plane to the display panel. The relationship between P_r^w and P_r^p can be described by Eq. (9):

$$z\begin{bmatrix} x_{\mathrm{er}}^a \\ y_{\mathrm{er}}^a \\ 1 \end{bmatrix} = K \cdot \begin{bmatrix} R & T \\ 0 & 1 \end{bmatrix} \begin{bmatrix} X_r^a \\ Y_r^a \\ z \\ 1 \end{bmatrix}. \tag{9}$$

In Eq. (9), K is the transformation matrix from the camera coordinate to the pixel coordinate; R and T represent the rotation matrix and translation matrix from the world coordinate to the camera coordinate, respectively. They can be acquired through camera calibration. Therefore, the determined eye position in the pixel coordinate can be transformed into the display coordinate, which can then be transformed into the corresponding backlight mode according to Eq. (7).

For autostereoscopic display, the view zone is actually a diamond-shaped area, as shown in Fig. 4. Therefore, viewing distance z is not always a fixed value. It fluctuates from $z_A = \frac{W^* z_{\mathrm{op}}}{W+E}$ to $z_B = \frac{W^* z_{\mathrm{op}}}{W-E}$, in which W is the length of the display panel, E is the width of the view zone, and z_{op} is the optimal viewing distance. Calculation error of the horizontal eye position due to the fluctuation of z can be determined by Eq. (10):

$$\Delta x = x_c - x_c' = \left(1 - \frac{z_{\mathrm{op}}}{z}\right) \times x_c, \tag{10}$$

where x_c and x_c' represent the actual and the calculated x coordinates of the eye position, respectively. The maximum of Δx is

$$\Delta x_{\max} = \left|\left(\frac{z_{\mathrm{op}}}{z_m} - 1\right) \times x_c\right|, \tag{11}$$

$$z_m = \begin{cases} z_A, & |z_A - z_{\mathrm{op}}| > |z_B - z_{\mathrm{op}}| \\ z_B, & \text{else} \end{cases}. \tag{12}$$

Later, in Section 3, it can be verified that for our prototype the calculation error Δx of the eye position due to a fixed z can be neglected.

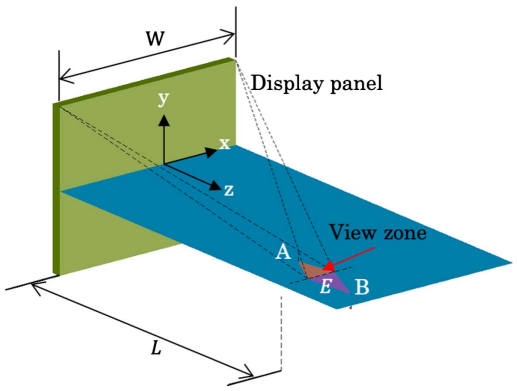

Fig. 4. Diamond-shaped area of view zone.

3. Experiments and Results

A bicylindrical lenticular lens is designed according to Eq. (1). By analyzing the parallelism of the light and the geometric modulation transfer function (MTF) of the bicylindrical lens, the optimization of the aberration can be verified. As shown in Fig. 5, we compare the simulation results of the customized lenslet and normal lenslet. The parallelism can be qualitatively judged by the radiation range on the observation plane. Figures 5(a) and 5(b) are the irradiance maps of the bicylindrical lens when the LED is at different positions. Despite the light attenuation, the distribution is similar on either the near or far observation plane. Figures 5(c) and 5(d) are the irradiance maps of the cylindrical lens when the LED is at different positions. It is obvious that the light distribution range becomes larger when it propagates to greater distance, when the LED is placed on the edge of the lens. However, when the LED is placed at the center of the lens, this divergence is not notable.

In addition, Fig. 5(e) is the normalized irradiance distribution of the parallel light by the bicylindrical lens and cylindrical lens when the LED is placed on the edge of the lens. As shown, the irradiance distribution is more even in the case of the bicylindrical lens than in the cylindrical lens case. By calculating the standard deviation of the flat top area, where the parallel light is mainly distributed, we can intuitively distinguish which one is more uniform. The standard deviation of the bicylindrical lens σ_a is 0.0220, and the deviation of the cylindrical lens σ_e is 0.0341, which is 1.55 times of σ_a. Also, the irradiance of the bicylindrical lens is higher than that of the cylindrical lens, meaning that the bicylindrical lens contributes to the improvement of efficiency. Figure 5(f) is the normalized irradiance distribution of the parallel light by the bicylindrical lens and cylindrical lens when the LED is placed at the center of the lens. As we can see, the distribution is not significantly different. The standard deviation of the flat top area is similar, where σ_c is 0.0116 for the bicylindrical lens, and σ_g is 0.0128 for the cylindrical lens. In Fig. 5(g), the irradiance distribution of different LED postures on the edge of the bicylindrical lens is shown. The standard deviation of the flat LED σ_i is 0.0406, which is 1.85 times of σ_a. According to the above analysis and data, it can be inferred that the bicylindrical lens with LEDs mounted on a curved surface can produce more evenly distributed parallel light with higher light efficiency.

The geometric MTF of the LLA1 unit is shown in Fig. 6. As shown in Figs. 6(a) and 6(b), they are the MTF curves of the bicylindrical lens and the cylindrical lens, respectively. In each figure, there are three curves that represent different off-axis distances. It is obvious that with the increase of the distance, the MTF decreases, both in the case of the bicylindrical lens and the cylindrical lens. However, the degree of reduction is weaker in the bicylindrical lens than in the cylindrical lens. As indicated in Figs. 6(c) and 6(d), when the off-axis distance is small, the difference of MTF is smaller, yet still there is a minor improvement from the cylindrical lens to the bicylindrical lens. When the off-axis distance is large, the improvement is rather significant.

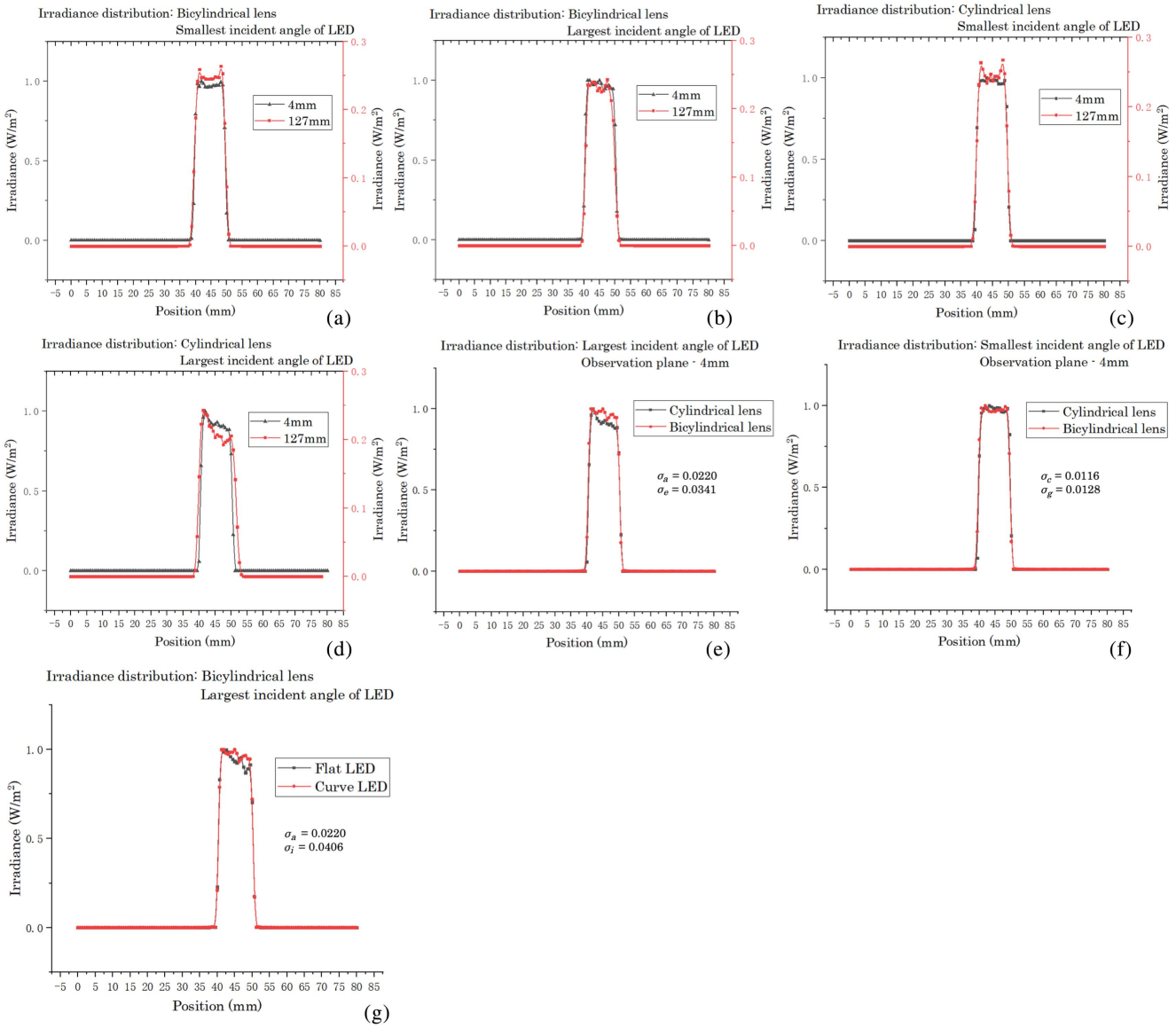

Fig. 5. Simulation result of LLA1.

In general, through the evaluation of the simulation result, our bicylindrical lens is indeed capable of better image quality.

A prototype based on the principle discussed above is set up, and the performance is verified through a series of experiments. Figure 7(a) shows the layout of the prototype, while Fig. 7(b) shows the structure of the designed bicylindrical lens. The LEDs are arranged on a curved surface as well, so the light efficiency of LLA1 can be improved when the LED is on the edge of LLA1. The backlight board is composed of 10 groups of LEDs, generating 10 different view zones as VZ1–VZ10. The characteristics of the LCD used in this prototype are summarized in Table 1. In the meantime, the parameters of LLA1 and LLA2 are recorded in Table 2. Polyethylene terephthalate (PET) is the optical interval between LLA1 and LLA2. The diffusion film is a special kind that only diffuses and uniforms the longitudinal brightness. In this way, the horizontal width of the light strip is strictly controlled.

In this prototype, S is set to be 60 mm, and the optimal viewing distance is 600 mm with maximal viewing angle of ±26 deg. Figure 7(c) is the outlook of our proposed autostereoscopic display system. The circled out module is the eye tracking device where only one RGB camera and one IR camera are used to detect the viewers' eye position.

After the eye tracking device detects and calculates eye positions, it transmits a BLCS to the BLCU. For our prototype, the calculating error of the eye position as mentioned in Eq. (10) can be determined. For the distance z that can provide proper autostereoscopic effects, according to Eqs. (11) and (12), $\Delta x_{\max} = 27$ mm, which is smaller than the half of S. Therefore, the calculating error of the eye position due to a fixed z_{op} can be neglected. According to Eqs. (7) and (9), the coordinate of the detected eye positions can be transformed to corresponding backlight mode. Considering that all optical elements are

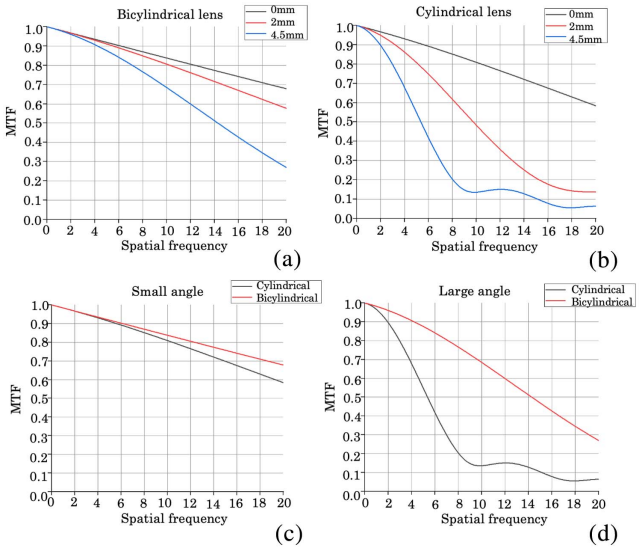

Fig. 6. Geometric MTF of the bicylindrical lens.

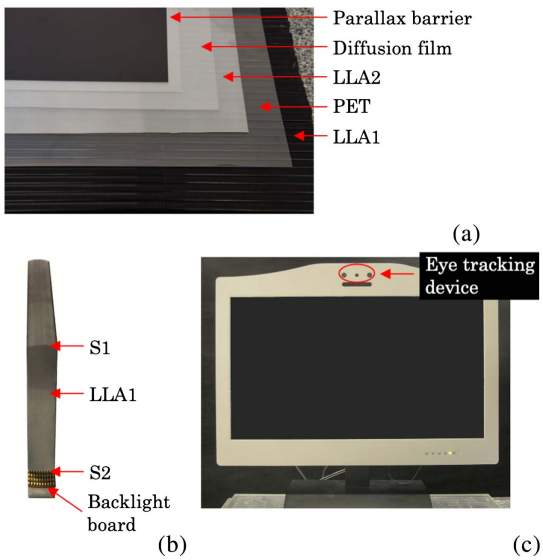

Fig. 7. Structure of the prototype. (a) Outlook of the prototype. (b) Bicylindrical lens. S1 and S2 are the two curved surfaces of LLA1. (c) Overall structure.

attached to each other with their centers aligned, the eye may not locate at the center of each view zone. Therefore, a more practical equation for Eq. (7) can be simplified as

$$X = -\beta_2\beta_1 x_i + \delta, \tag{13}$$

where X is the display coordinate of the eye position, i is the group number of the LED, β_1, β_2 are the magnified factors mentioned earlier, and $-30 < \delta < 30$.

For example, Fig. 8 demonstrates the effect of displaying the left image and right image that are projected to two neighboring spatial locations [Figs. 8(a) and 8(b) for VZ5, Figs. 8(c) and 8(d) for VZ6] by the directional backlight alternately. As we can see

Table 1. Specifications for the LCD Panel.

Parameter	Value
Screen diagonal	27 in.
Resolution in 3D mode	1920 × 1080
Response time	5 ms (Typ. on/off)
Frame rate	120 Hz

Table 2. Parameters for the Two Lens Arrays.

	LLA1 (mm)	LLA2 (mm)
Pitch	10	0.18293
Focal length	32.8	0.6
Radius of S1	16.4	0.3
Radius of S2	25.8	–

in Figs. 8(a) and 8(c), at both positions, the images can be seen clearly, indicating that the crosstalk is rather small. In Figs. 8(b) and 8(d), the displayed image is pure white with the corresponding backlight on and the rest off. The white band is where the corresponding view zone locates, and the rest of the places are dark.

Crosstalk is one of the most critical parameters for autostereoscopic display. For the proposed autostereoscopic display scheme, the crosstalk can be calculated by Eq. (14):

$$\mathrm{CT}_i = \frac{\sum_{n\neq i} I_n}{I_i} \times 100\%, \tag{14}$$

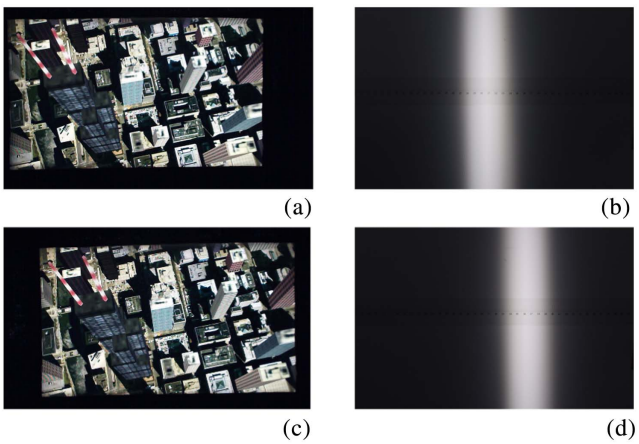

Fig. 8. In (a) and (c), the LCD is displaying the left and right building images, respectively. In (b) and (d), the LCD is displaying the pure white image and the directional backlight projects light to the corresponding view zone at the optimal viewing distance.

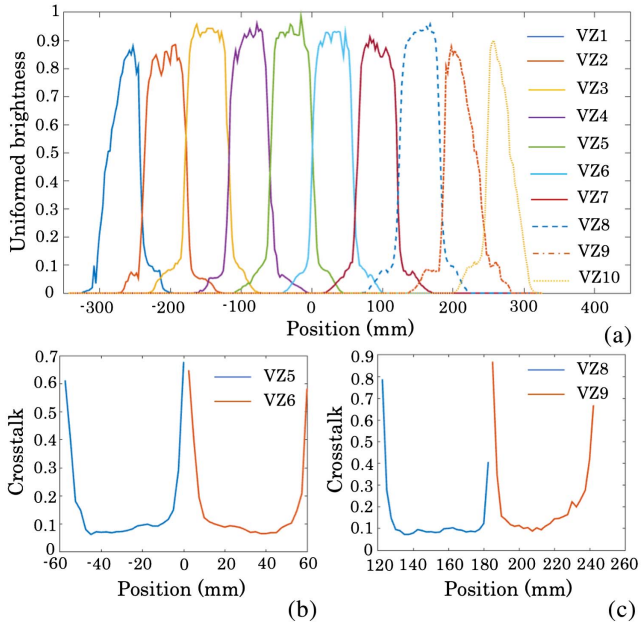

Fig. 9. Crosstalk evaluation. (a) Light distribution for 10 views. (b) Crosstalk for the two middle view zones (VZ5 and VZ6). (c) Crosstalk for VZ8 and VZ9 with large viewing angle.

in which CT_i refers to the crosstalk for the ith view zone, $\sum_{n\neq i} I_n$ is the total leaking luminance at the ith view zone contributed by all the other view zones, and I_i is the desired luminance of the ith view zone. As shown in Fig. 9(a), the light distribution is measured by a luminometer every 2.5 mm at the optimal viewing distance. It is measured by displaying a pure white image, while only turning on the corresponding backlight. As we can see, with the bicylindrical lens, when the viewing angle increases, the brightness of the exit pupil decreases slightly. Figure 9(b) is the crosstalk of VZ5 and VZ6, where the minimal crosstalk is 6%. Actually, there are several different display modes considering that the eyes are located at different positions, and crosstalk for VZ5 and VZ6 represents the most common scenario when the viewer's left eye locates at VZ5 and right eye at VZ6. The crosstalk for VZ5 is mainly contributed by VZ6 and VZ4, and VZ5 and VZ7 for VZ6.

With the increase of the viewing angle to 20 deg, such as VZ8 and VZ9, the crosstalk is increased to 8.8%, which is shown in Fig. 9(c). The distribution of the viewing zone at a large angle is sharply distributed with a slightly smaller slope. These two features undermine the display effect regarding contrast and crosstalk. The crosstalk for VZ8 is mainly contributed by VZ7 and VZ9, and the crosstalk for VZ9 is mainly contributed by VZ8 and VZ10. However, this result is much better compared to the autostereoscopic display system based on a parallax barrier or lenticular lens.

With the increase of the viewing angle, the brightness gradually decreases. The brightness difference between adjacent view zones is 10%. This may not spoil the viewing experience. But, for future perfection, the local backlight control strategy can be adopted.

Here, the performance of our system is summarized in Table 3, together in comparison with other kinds of display systems. As we can see from the table, the viewing angle of our system is improved compared with that of the free-form surface backlight (FFSB) system[1] and parallax barrier system. Also, the crosstalk at the central viewing zone is lower. The overall performance is better than the traditional system based on the parallax barrier. However, by measuring the brightness of each viewing zone, the average brightness in 3D mode is 103.5 cd/m^2 for our prototype. The efficiency of the system is low due to the small light aperture of the parallax barrier, which is in need of replacement for future improvement.

4. Conclusion

In this paper, an autostereoscopic 3D display system based on the spatial-temporal multiplexing technique is introduced. The system consists of a directional backlight module, BLCU, LCD panel of high refreshing rate, and eye tracking device. The directional backlight module, which forms view zones at specific locations, comprises LLA1 with larger pitch and LLA2 with smaller pitch, LEDs that are divided into 10 groups, a parallax barrier, and other optical films. To correct optical aberration and form light strips with smaller width, especially for large viewing angle, LLA1 is designed to be a bicylindrical

Table 3. Summary of the System Performance.

	Viewing Angle	Crosstalk	Luminance/Efficiency
Our system	±26 deg	6% at the central viewing angle, 8.8% at large viewing angle	103.5 cd/m^2/10% in 3D mode
System1 with FFSB	±23 deg	7.39% at the central viewing angle	304 cd/m^2/–
System2 with parallax barrier	±12 deg	10%–15%	–/20%
System3 with micro-projection dynamic backlight[20]	±12 deg	–	–
System4 with lenticular sheet and liquid crystal parallax barrier[11]	±28.8 deg	Average crosstalk 17.1%	–

lens. The LEDs are arranged on a curved surface so that the light efficiency can be improved when it is on the edge of LLA1. Still, the light efficiency is decreased a little when the viewing angle is large, because light can be absorbed by the parallax barrier. However, to make the exit pupil distribution more even, locally controllable backlight can be adopted in our future work. Composed of a long-wavelength IR camera and a visible spectrum camera, the eye tracking device detects the eye positions with faster speed, transforms them to a corresponding backlight mode, and transmits the mode information to the BLCU. A prototype based on our optical design is set up, and relevant experiments are carried out to verify the feasibility. The minimal crosstalk is 6%, and viewing angle is increased to ±26 deg.

References

1. H. Fan, Y. Zhou, J. Wang, H. Liang, P. Krebs, J. Su, D. Lin, K. Li, and J. Zhou, "Full resolution, low crosstalk, and wide viewing angle auto-stereoscopic display with a hybrid spatial-temporal control using free-form surface backlight unit," J. Disp. Technol. **11**, 620 (2015).
2. A. K. Srivastava, J. L. de Bougrenet de la Tocnaye, and L. Dupont, "Liquid crystal active glasses for 3D cinema," J. Disp. Technol. **6**, 522 (2010).
3. M. Lambooij, W. Ijsselsteijn, M. Fortuin, and I. Heynderickx, "Visual discomfort and visual fatigue of stereoscopic displays: a review," J. Imaging Sci. Technol. **53**, 30201 (2009).
4. S. Lee, J. Kim, and S. Lee, "Behavioral circuit models of stereoscopic 3-D liquid crystal displays and shutter glasses," IEEE Trans. Electron Dev. **62**, 3302 (2015).
5. K. Yoon, H. Ju, H. Kwon, I. Park, and S. Kim, "Diffraction effects incorporated design of a parallax barrier for a high-density multi-view autostereoscopic 3D display," Opt. Express **24**, 4057 (2016).
6. G. Lv, Q. Wang, J. Wang, and W. Zhao, "Multi-view 3D display with high brightness based on a parallax barrier," Chin. Opt. Lett. **11**, 121101 (2013).
7. G. Lv, J. Wang, W. Zhao, and Q. Wang, "Three-dimensional display based on dual parallax barriers with uniform resolution," Appl. Opt. **52**, 6011 (2013).
8. X. Yu, X. Sang, D. Chen, P. Wang, X. Gao, T. Zhao, B. Yan, C. Yu, D. Xu, and W. Dou, "3D display with uniform resolution and low crosstalk based on two parallax interleaved barriers," Chin. Opt. Lett. **12**, 121001 (2014).
9. S. Lee, J. Park, J. Heo, B. Kang, D. Kang, H. Hwang, J. Lee, Y. Choi, K. Choi, and D. Nam, "Autostereoscopic 3D display using directional subpixel rendering," Opt. Express **26**, 20233 (2018).
10. L. Qi, Q. Wang, J. Luo, W. Zhao, and C. Song, "An autostereoscopic 3D projection display based on a lenticular sheet and a parallax barrier," J. Disp. Technol. **8**, 397 (2012).
11. X. Ma, W. Zhao, J. Hu, G. Lv, and Q. Wang, "Autostereoscopic three-dimensional display with high resolution and low cross talk using a time-multiplexed method," Opt. Eng. **57**, 095105 (2018).
12. Y. Takaki, "Multi-view 3-D display employing a flat-panel display with slanted pixel arrangement," J. Soc. Inf. Display **18**, 476 (2010).
13. L. Qi, Q. Wang, J. Luo, A. Wang, and D. Liang, "Autostereoscopic 3D projection display based on two lenticular sheets," Chin. Opt. Lett. **10**, 011101 (2012).
14. K. Chien and H. D. Shieh, "Time-multiplexed three-dimensional displays based on directional backlights with fast-switching liquid-crystal display," Appl. Opt. **45**, 3106 (2006).
15. C. Chen, Y. Yeh, and H. D. Shieh, "3-D mobile display based on Moire-free dual directional backlight and driving scheme for image crosstalk reduction," J. Disp. Technol. **4**, 92 (2008).
16. H. Liang, S. An, J. Wang, Y. Zhou, H. Fan, P. Krebs, and J. Zhou, "Optimizing time-multiplexing auto-stereoscopic displays with a genetic algorithm," J. Disp. Technol. **10**, 695 (2014).
17. J. Wang, H. Liang, H. Fan, Y. Zhou, P. Krebs, J. Su, Y. Deng, and J. Zhou, "High-quality autostereoscopic display with spatial and sequential hybrid control," Appl. Opt. **52**, 8549 (2013).
18. D. Miyazaki, Y. Hashimoto, T. Toyota, K. Okoda, T. Okuyama, T. Ohtsuki, A. Nishimura, and H. Yoshida, "Multi-user autostereoscopic display based on direction-controlled illumination using a slanted cylindrical lens array," Proc. SPIE **9011**, 90111G (2014).
19. B. Xu, Q. Wu, Y. Bao, G. Chen, Y. Wang, and S. Ren, "Time-multiplexed stereoscopic display with a quantum dot-polymer scanning backlight," Appl. Opt. **58**, 4526 (2019).
20. B. Zhao, R. Huang, and G. Lv, "Micro-projection dynamic backlight for multi-view 3D display," Chin. Opt. Lett. **19**, 092201 (2021).